Controllable lateral optical force in a double-sphere system

Junxuan Wang,[1] Yaxin Li,[1] Xiao Li,[2] Lei Zhang,[3,4,*] and Jun Chen[1,4,†]

[1]*State Key Laboratory of Quantum Optics and Quantum Optics Devices, Institute of Theoretical Physics, Shanxi University, Taiyuan 030006, China*

[2]*Department of Physics, The Hong Kong University of Science and Technology, Hong Kong 999077, China*

[3]*State Key Laboratory of Quantum Optics and Quantum Optics Devices, Institute of Laser Spectroscopy, Shanxi University, Taiyuan 030006, China*

[4]*Collaborative Innovation Center of Extreme Optics, Shanxi University, Taiyuan 030006, China*

(Received 15 January 2024; accepted 17 April 2024; published 6 May 2024)

Extensive studies have been conducted on the lateral optical force, which is perpendicular to the direction of light propagation. Current research is primarily focused on the lateral force experienced by a single sphere. In this study, we investigate the lateral optical force exerted on a double-sphere system aligned along the direction of evanescent-wave propagation, utilizing full-wave simulations and the multipole-expansion method. Despite no apparent lateral asymmetry, we find that each sphere can experience either positive or negative lateral optical force by tuning the incident wave's frequency and polarization. Unlike the lateral force experienced by a single sphere in an evanescent wave, arising solely from recoil force due to Belinfante's spin momentum in a circularly polarized evanescent wave or spin angular momentum in a linearly diagonally polarized evanescent wave, the lateral force exerted on each sphere in the double-sphere system can also stem from an interception force. This interception force occurs due to the field gradient caused by the spheres' asymmetric scattering. This asymmetry is rooted in the real or imaginary part of the complex Poynting vector of the incident wave. It is the interception force that enables continuous tuning of the lateral optical force of each sphere and their sign flip. This research advances the understanding of lateral optical force and offers more flexibility for optical manipulation in multiparticle systems, opening up new opportunities for lateral-force-based applications.

DOI: 10.1103/PhysRevA.109.053505

I. INTRODUCTION

Lateral optical forces [1–9], acting perpendicular to light propagation, have received considerable attention. One concept possessing a pertinent feature with this is the lateral optical gradient force, which is caused by the field gradient and is observed in applications such as transversely trapping particles on the optical axis in optical tweezers [10–14] and confining particles near the surface of optical fibers [15,16]. However, lateral optical forces are defined in a direction where the incident light does not have a field gradient. Such forces can result from some form of asymmetry, such as the inherent asymmetry in chiral structures [1,17] and materials [18–22]. Interestingly, lateral optical forces can persist even when there is no apparent left-right asymmetry in both the incident optical field and the illuminated particle [2–4,7–9,23–30]. For instance, these forces can emerge from the breaking of electric-magnetic symmetry [28], scattering asymmetry induced by spin-orbit coupling [3,4,23,27], Belinfante's spin momentum (BSM) resulting from the real part of the complex Poynting vector in a circularly polarized evanescent wave [2], and the transverse spin angular momentum (SAM) proportional to the transverse imaginary Poynting vector in a linearly diagonally polarized evanescent wave [8].

Current research on lateral optical forces is primarily focused on a single particle. However, many systems consist of multiple particles, which can be used in various applications such as biological studies [31], colloidal assembly [32], quantum technologies [33], imaging techniques [34], and microscale engineering [35,36]. Given the significant role of the lateral force in optical manipulation within multiparticle systems, it is intriguing and necessary to investigate the lateral optical force in these systems.

In this work, we study the lateral optical forces exerted on a double-sphere system aligned along the direction of evanescent-wave propagation. Neither the incident beam nor the double-sphere system shows any apparent lateral asymmetry [see Fig. 1(a) for an example]. Through comprehensive analysis with full-wave simulations and multipole-expansion theory, we discover that the lateral optical forces exerted on each sphere in a double-sphere system are contributed not only by the recoil force but also by an interception force. This is unlike a single-sphere system. The interception force originates from the transverse field gradient, which is caused by asymmetric scattering between the spheres. The asymmetric scattering of an isotropic sphere arises from the inherently asymmetrical real part of the complex Poynting vector of the incident circularly polarized evanescent wave or the asymmetrical imaginary part in the case of linearly

*zhanglei@sxu.edu.cn
†chenjun@sxu.edu.cn

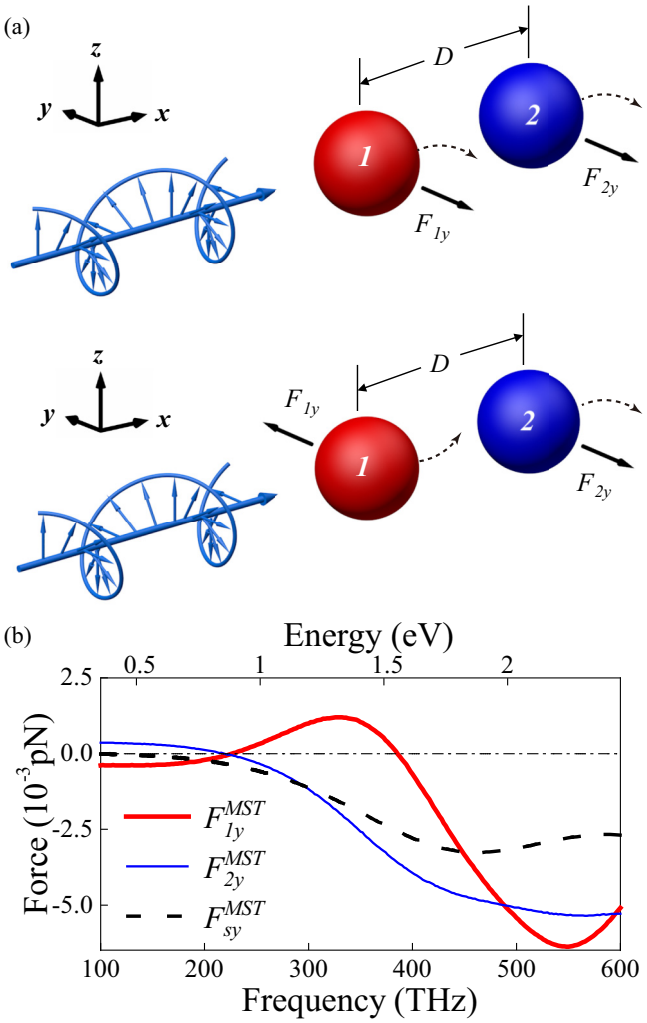

FIG. 1. (a) Schematic plot of a double-sphere system. It involves two identical spheres in the field of a circularly polarized evanescent wave. This wave propagates along the x direction and decays in the $z > 0$ half-space. The two spheres can move laterally in the same or opposite directions due to the lateral optical force. In the calculations for this paper, the coordinates for spheres 1 and 2 are set as $(-D, 0, \lambda/2)$ and $(0, 0, \lambda/2)$, respectively. The two spheres are aligned in the direction of propagation, with a separation distance of D. However, as the incident evanescent wave is uniformly distributed on the xy plane, the position of the two spheres on the $z = \lambda/2$ plane does not affect the results. The outcome remains the same as long as the relative positions of the two spheres are consistent. (b) The lateral optical force exerted on the first (F_{1y}^{MST}, red thick line) and second (F_{2y}^{MST}, blue thin line) gold spheres in the double-sphere system versus the frequency and energy. The incident light is a circularly polarized evanescent wave ($p = \sqrt{2}/2, q = \sqrt{2}i/2$). For comparison, the lateral force on a single gold sphere is shown by the black dashed line (F_{sy}^{MST}). The center-to-center distance in the double-sphere system is $D = 0.4$ μm.

diagonally polarized evanescent waves. Interestingly, this interception force can cause the lateral optical forces on the two spheres to point in either the same or opposite directions. This flexibility could potentially enable the adjustment of the direction of lateral optical forces in a system involving multiple spheres. Moreover, in a linearly diagonally polarized evanescent wave, the lateral optical forces exerted on the two spheres are less tunable with scattering compared to those in a circularly polarized evanescent wave. This is attributed to the less pronounced asymmetric scattering in a linearly diagonally polarized evanescent wave. Our findings can be extended to systems composed of more spheres.

II. SYSTEM SETTINGS AND THEORETICAL FORMALISM

We consider a double-sphere system in a single evanescent wave, as illustrated in Fig. 1(a). This system consists of two identical gold spheres. They are aligned in the direction of the evanescent-wave propagation and situated at $z = \lambda/2$. Each sphere has a radius of $r = 0.1$ μm, and the distance between their centers is denoted as D. The permittivity of gold is modeled by the Drude model, $\varepsilon_r = 1 - \omega_p^2/(\omega^2 + i\omega\gamma)$, with the plasmonic frequency given as $\omega_p = 1.37 \times 10^{16}$ rad/s (corresponding to a photon energy of 8.995 eV) and the damping frequency given as $\gamma = 4.084 \times 10^{13}$ rad/s (corresponding to a photon energy of 2.668×10^{-2} eV) [37]. The electric field of the evanescent wave, which propagates along the x axis and decays in the $z > 0$ half-space, can be expressed as follows [8]:

$$\mathbf{E}^{\mathrm{inc}} = E_0\left[\frac{i\kappa}{k_x}p\hat{\mathbf{x}} + \frac{k}{k_x}q\hat{\mathbf{y}} - p\hat{\mathbf{z}}\right]e^{ik_x x - \kappa z}, \tag{1}$$

in which the time dependence $e^{-i\omega t}$ has been assumed and omitted for simplicity. E_0 represents the amplitude of the electric field at $z = 0$. The complex numbers p and q define the polarization state, normalized by $|p|^2 + |q|^2 = 1$. For instance, TM polarization is defined by $p = 1$ and $q = 0$. TE polarization is defined by $p = 0$ and $q = 1$. Diagonal linear polarization (DLP) is defined by $p = q = \sqrt{2}/2$. Circular polarization (CP) is defined by $p = \sqrt{2}/2, q = \pm\sqrt{2}i/2$. The wave number is denoted by k, the longitudinal wave number is denoted by k_x, and the exponential decay rate is denoted by κ. They satisfy the equation $k^2 = k_x^2 - \kappa^2$, and the complex wave vector is denoted by $\mathbf{k} = k_x\hat{\mathbf{x}} + i\kappa\hat{\mathbf{z}}$. In this paper, the exponential decay rate is set to $\kappa = 0.1k$, and $E_0 = 10^6$ V/m.

Here, we use two methods to calculate the time-averaged optical force exerted on the two spheres. On the one hand, the optical forces $\mathbf{F}^{\mathrm{MST}}$ exerted on the two spheres are numerically obtained by integrating the Maxwell stress tensor on a closed surface around each sphere [38]. The total optical fields are computed using full wave simulation via COMSOL MULTIPHYSICS. On the other hand, for a better understanding of the complex lateral optical force behavior in the double-sphere system, we employ the multipole expansion of optical forces [39]. The optical force $\mathbf{F}^{\mathrm{MUL}}$ exerted on a particle in any monochromatic optical field can be described as a sum of the interception (extinction) force $\mathbf{F}^{\mathrm{int}}$ and the recoil force $\mathbf{F}^{\mathrm{rec}}$ [40–43]:

$$\mathbf{F}^{\mathrm{MUL}} = \mathbf{F}^{\mathrm{int}} + \mathbf{F}^{\mathrm{rec}}. \tag{2}$$

The interception force $\mathbf{F}^{\mathrm{int}}$ originates from the interaction between electric (magnetic) multipoles of different orders induced on the particle and the incident electric (magnetic) field.

Physically, it can be seen as the momentum transferred from the incident photons to the particle during light-scattering interception. The recoil force $\mathbf{F}^{\text{rec}}$ arises from the interaction between the induced multipoles on the particle. It can also be interpreted as the momentum gained by the particle during the scattering reradiation process when the induced multipoles reemit light. In other words, per the principle of momentum conservation, particles will gain or lose momentum during the reemission of light by excited multipoles. This momentum change results in the particles experiencing a recoil force. Since this involves a continuous change in the momentum state of the particles, it is a dynamic physical process. Here, we express $\mathbf{F}^{\text{int}}$ and $\mathbf{F}^{\text{rec}}$ in terms of the dominant multipoles up to the electric quadrupole order [42,44]:

$$\mathbf{F}^{\text{int}} = \mathbf{F}^{\mathbf{p}} + \mathbf{F}^{\mathbf{m}} + \mathbf{F}^{\mathbf{Q}}, \quad \mathbf{F}^{\text{rec}} = \mathbf{F}^{\mathbf{pm}} + \mathbf{F}^{\mathbf{Qp}}, \tag{3}$$

where

$$\begin{aligned}
\mathbf{F}^{\mathbf{p}} &= \frac{1}{2}\text{Re}[(\nabla \mathbf{E}^*)\cdot\mathbf{p}],\\
\mathbf{F}^{\mathbf{m}} &= \frac{1}{2}\text{Re}[(\nabla \mathbf{B}^*)\cdot\mathbf{m}],\\
\mathbf{F}^{\mathbf{Q}} &= \frac{1}{4}\text{Re}\big[(\nabla\nabla \mathbf{E}^*):\mathbf{Q}^{(e)}\big],\\
\mathbf{F}^{\mathbf{pm}} &= -\frac{k^4}{12\pi\varepsilon_0 c}\text{Re}[\mathbf{p}\times\mathbf{m}^*],\\
\mathbf{F}^{\mathbf{Qp}} &= -\frac{k^5}{40\pi\varepsilon_0}\text{Im}\big[\mathbf{Q}^{(e)}\cdot\mathbf{p}^*\big].
\end{aligned} \tag{4}$$

$\mathbf{p}$, $\mathbf{m}$, and $\mathbf{Q}^{(e)}$ represent the electric dipole, magnetic dipole, and electric quadrupole moments, respectively [39]. $\mathbf{E}$ and $\mathbf{B}$ represent the total incident electric and magnetic fields acting on the particle. They can be expressed as $\mathbf{E} = \mathbf{E}^{\text{inc}} + \mathbf{E}^{\text{sca}}$ and $\mathbf{B} = \mathbf{B}^{\text{inc}} + \mathbf{B}^{\text{sca}}$, where $\mathbf{E}^{\text{inc}}$ and $\mathbf{B}^{\text{inc}}$ are the initial incident evanescent fields, while $\mathbf{E}^{\text{sca}}$ and $\mathbf{B}^{\text{sca}}$ are the fields scattered by the other particle. When the particle size is significantly smaller than the wavelength, $\mathbf{E}^{\text{sca}}$ and $\mathbf{B}^{\text{sca}}$ can be approximated using the electric and magnetic dipole fields [38,45]:

$$\begin{aligned}
\mathbf{E}^{\text{sca}} &= \frac{1}{4\pi\varepsilon_0}\Bigg\{k^2(\mathbf{n}\times\mathbf{p})\times\mathbf{n}\frac{e^{ikr'}}{r'}\\
&\quad +[3\mathbf{n}(\mathbf{n}\cdot\mathbf{p})-\mathbf{p}]\left(\frac{1}{r'^3}-\frac{ik}{r'^2}\right)e^{ikr'}\Bigg\}\\
&\quad -\frac{Z_0k^2}{4\pi}(\mathbf{n}\times\mathbf{m})\frac{e^{ikr'}}{r'}\left(1-\frac{1}{ikr'}\right),\\
\mathbf{B}^{\text{sca}} &= \frac{\mu_0 ck^2}{4\pi}(\mathbf{n}\times\mathbf{p})\frac{e^{ikr'}}{r'}\left(1-\frac{1}{ikr'}\right)\\
&\quad +\frac{\mu_0}{4\pi}\Bigg\{k^2(\mathbf{n}\times\mathbf{m})\times\mathbf{n}\frac{e^{ikr'}}{r'}\\
&\quad +[3\mathbf{n}(\mathbf{n}\cdot\mathbf{m})-\mathbf{m}]\left(\frac{1}{r'^3}-\frac{ik}{r'^2}\right)e^{ikr'}\Bigg\},
\end{aligned} \tag{5}$$

where $Z_0 = \sqrt{\mu_0/\varepsilon_0}$ represents the impedance of the free space, $r' = |\mathbf{r}'|$ stands for the radial distance, and $\mathbf{n}$ denotes a unit vector in the direction of $\mathbf{r}'$.

III. CIRCULARLY POLARIZED EVANESCENT-WAVE CASE

In this section, we consider the case in which the incident evanesce wave is circularly polarized ($p = \sqrt{2}/2$, $q = \sqrt{2}i/2$). The lateral optical force directly calculated from Maxwell's theory F_y^{MST} is shown in Fig. 1(b). It is interesting that the direction of the lateral force exerted on each sphere in the double-sphere system can be along either the $+y$ or $-y$ direction, depending on the incident wave's frequency. More importantly, the two spheres can move laterally in the same or opposite directions due to the lateral force [see Fig. 1(b) and the schematic diagrams in Fig. 1(a)]. In contrast, for a single sphere in the same evanescent wave, the sphere can experience a lateral force only in the $-y$ direction (F_{sy}), as shown by the black dashed line, which is induced by BSM [2,8].

To understand the intriguing behavior of lateral forces in the double-sphere system, we resort to the multipole expansion of optical forces [Eqs. (2)–(4)]. The results from these two methods align perfectly for a single sphere in an evanescent wave, as seen by the black solid line and the red circles in Fig. 2(a). Furthermore, for the double-sphere system, the results from both methods agree well with each other and have only a small deviation at high frequencies, as shown in Figs. 2(b) and 2(c). This discrepancy mainly stems from the use of Eq. (5) to describe the fields scattered by the other sphere when using the multipole-expansion equations of the interception force in Eq. (4). At short wavelengths, the other sphere can no longer be viewed as a dipole.

For a single-sphere system, the interception force F_{sy}^{int} is completely zero due to the incident field intensity's uniformity on the xy plane. Consequently, the lateral optical force on the sphere originates entirely from the recoil force F_{sy}^{rec}, as shown in Fig. 2(a). This lateral optical force has been proven to be induced entirely by BSM [2,8], which stems from the asymmetrical real part of the incident evanescent wave's complex Poynting vector in the lateral y direction [see the white arrows in Fig. 2(d)]. However, the interception force can play a determinative role in changing the lateral force's sign in the double-sphere system presented in Figs. 2(b) and 2(c). In the following, we will analyze the interception force in the double-sphere system in detail.

In comparison, the nonzero interception force F_y^{int} of one sphere in the double-sphere system results from the asymmetric scattering from the other sphere. Figure 2(e) presents the scattered field intensity of a single sphere with asymmetric distribution along the y axis. For a clearer view, we illustrate the normalized field magnitude of the scattered light at $x = -0.4$ μm on the sphere's left side. It shows that the light scattering tends to propagate in the $+y$ direction, as demonstrated in Fig. 2(f). In fact, this asymmetry stems from the real part of the incident evanescent wave's complex Poynting vector along the y direction [46].

Moreover, we find that the direction of the interception force resulting from the spheres' mutual scattering can be modified by the incident evanescent wave's frequency. As shown in Figs. 2(b) and 2(c), its direction can be positive or negative, causing the total lateral force exerted on the sphere to change direction with frequency. The interception force's direction dependence on the frequency can be understood

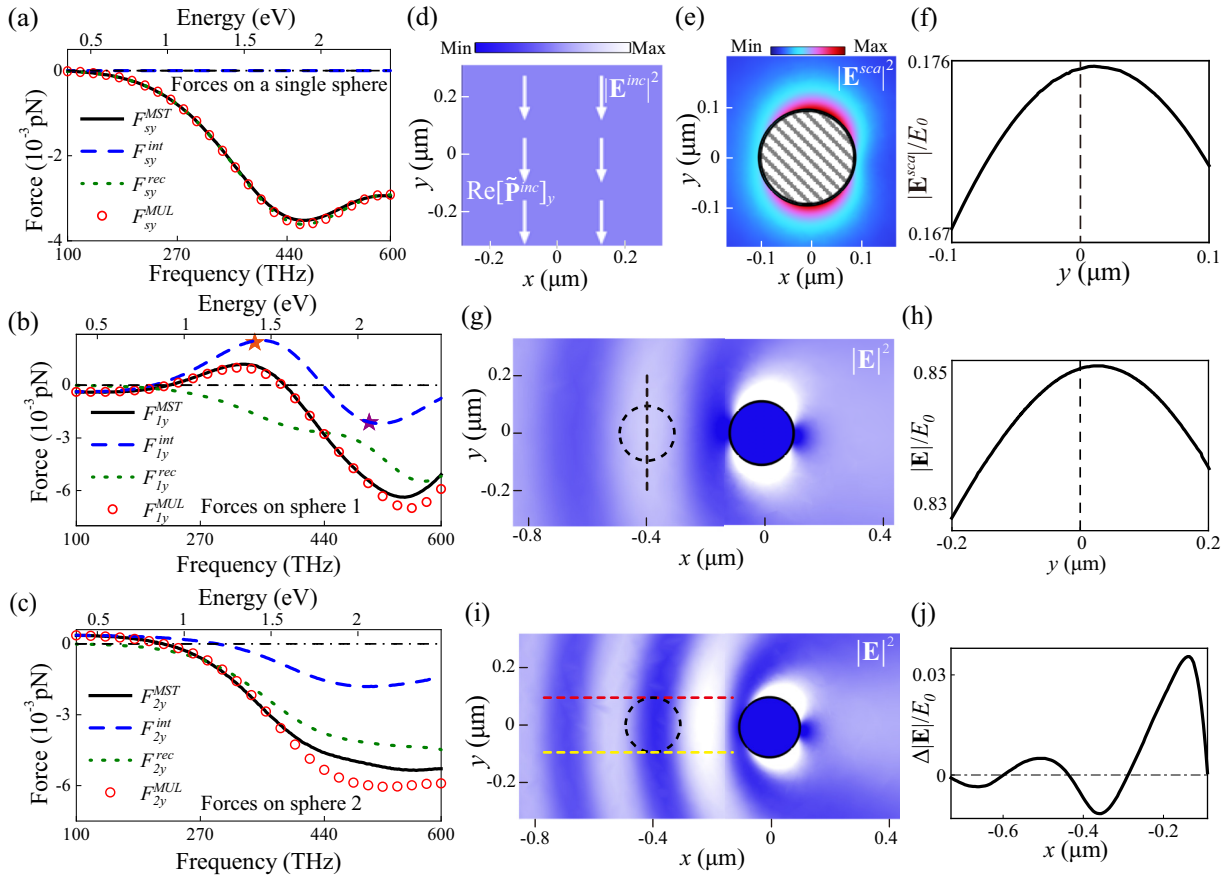

FIG. 2. (a)–(c) Lateral optical forces exerted on a single sphere or the two spheres in a double-sphere system versus frequency and energy. These forces are calculated directly from Maxwell's theory (F_y^{MST}) or through the multipole expansion of optical forces (F_y^{MUL}, F_y^{int}, F_y^{rec}). (d) The uniform intensity of the incident evanescent wave on the xy plane. The white arrows represent the y component of the real part of the incident evanescent wave's complex Poynting vector. (e) The intensity of the field scattered from a gold sphere (represented by the gray stripes), with an incident wave frequency of 350 THz. (f) The normalized scattered field magnitude along the y direction to the left of the gold sphere at $x = -0.4$ μm. (g) and (i) The total electric field computed using a full-wave simulation in the presence of a gold sphere (indicated by a solid black circle) with incident-wave frequencies of 350 and 510 THz, respectively. (h) The normalized magnitude of the electric field at the vertical black dashed line in (g). (j) The difference between the electric-field magnitude at the upper red and lower yellow dashed lines in (i). The center-to-center distance in the double-sphere system is $D = 0.4$ μm. The incident light is a circularly polarized evanescent wave ($p = \sqrt{2}/2, q = \sqrt{2}i/2$).

by examining the distribution of the total incident optical field **E**. As depicted in Figs. 2(g) and 2(i) (corresponding to frequencies of 350 and 510 THz, respectively), the incident evanescent wave striking a gold sphere (outlined by the black solid circle) interferes with the backward scattered light, producing distinct interference fringes in the sphere's left area [38,47]. However, there are no apparent interference fringes in the sphere's right area. Thus, in the system shown in Fig. 1(a), sphere 1 is more significantly affected by the interference field. However, sphere 2 is less affected by the interference field, so the behavior of its lateral force versus frequency is similar to that of a single sphere [shown in Figs. 2(a) and 2(c)]. Next, we analyze the sign change of F_{1y}^{int} on sphere 1 shown by the orange and purple stars in Fig. 2(b). When analyzing the force exerted on sphere 1, we consider only the dominant first scattering by sphere 2. This refers to the light scattered to sphere 1 after the incident light hits sphere 2, disregarding any multiple scattering between the two spheres. Sphere 1 (marked by the black dashed circle) is placed in the total incident field composed of the incident evanescent wave and the scattered field from sphere 2 in Figs. 2(g) and 2(i). When the frequency of the incident evanescent wave is 350 THz, sphere 1 is situated in the bright fringe depicted in Fig. 2(g). In addition, the magnitude of the electric field along the vertical black dashed line is shown in Fig. 2(h). It is evident that the peak of the electric-field magnitude is skewed toward the $+y$ direction. As a result of the field gradient, sphere 1 experiences an F_{1y}^{int} directed toward the $+y$ direction. However, as shown in Fig. 2(i), when the frequency of the incident evanescent wave is 510 THz, sphere 1 is situated in the dark fringe. Figure 2(j) highlights the difference between the electric-field magnitude at the upper red dashed line and that at the lower yellow dashed line in Fig. 2(i), indicating that the field magnitude on the lower side of sphere 1 is stronger than that on the upper side at $x = -0.4$ μm. This results in sphere 1 experiencing an interception force in the $-y$ direction. Additionally, Fig. 2(j) reveals a pattern: in the dark fringe, the field magnitude at $y < 0$ is

stronger than the field magnitude at $y > 0$ (the difference is negative), while in the bright fringe, the field magnitude at $y > 0$ is stronger than the field magnitude at $y < 0$ (the difference is positive). It can be understood as follows. The bright fringe is a result of the superposition between the wave peaks (or troughs) from both the incident evanescent wave and the backward-scattering wave from sphere 2. Conversely, the dark fringe results from the superposition between their wave peaks and troughs. On the left side of sphere 2, the backward scattering tends to laterally propagate in the $+y$ direction. Therefore, the magnitude or amplitude of the scattered wave in the $y > 0$ area is greater than that in the $y < 0$ area. At the bright fringe, the electric-field amplitude in the $y > 0$ area is the sum of the uniform incident-wave amplitude and the relatively large scattering-wave amplitude. Therefore, it exceeds the sum of the incident-wave amplitude and the relatively small scattering-wave amplitude in the $y < 0$ area. However, at the dark fringe, the electric-field amplitude in the $y > 0$ area is the difference between the incident-wave amplitude and the relatively large scattering-wave amplitude. Hence, it is less than the difference between the incident-wave amplitude and the relatively small scattering-wave amplitude in the $y < 0$ area, as depicted in Fig. 2(j). Thus, we can conclude that adjusting the frequency, which effectively tunes the interference fringe, changes the field-intensity distribution along the lateral y direction. This enables us to alter the direction of the lateral optical force exerted on the sphere.

Therefore, the lateral optical force exerted on each sphere is actually the competition between BSM and the scattering between the two spheres. At low frequencies, the interception force induced by the scattering mechanism dominates. This is due to the distance between the spheres being significantly smaller than the wavelength, which enhances scattering. To investigate this effect, we further reduce the distance between spheres from $D = 0.4$ μm to $D = 0.3$ μm. The results are presented in Fig. 3. It is found that the closer sphere separation results in opposite directions of lateral forces for the two spheres over a larger frequency range, particularly at low frequencies. The lateral forces on the two spheres are nearly equal in magnitude but opposite in direction due to strong mutual scattering. One can visualize this as the photons scattered by the first sphere pushing the second sphere to move in the $+y$ direction while simultaneously receiving a recoil in the $-y$ direction. As frequency increases, similar to what happens when increasing the sphere separation relative to the wavelength, the mutual scattering weakens. This allows the lateral optical force induced by BSM mechanism to become apparent and even dominant, as shown by the green dotted lines in Figs. 2(b), 2(c), 3(b), and 3(c). This results in the lateral forces exerted on the two spheres being in the same direction, as seen in Figs. 1(b) and 3(a).

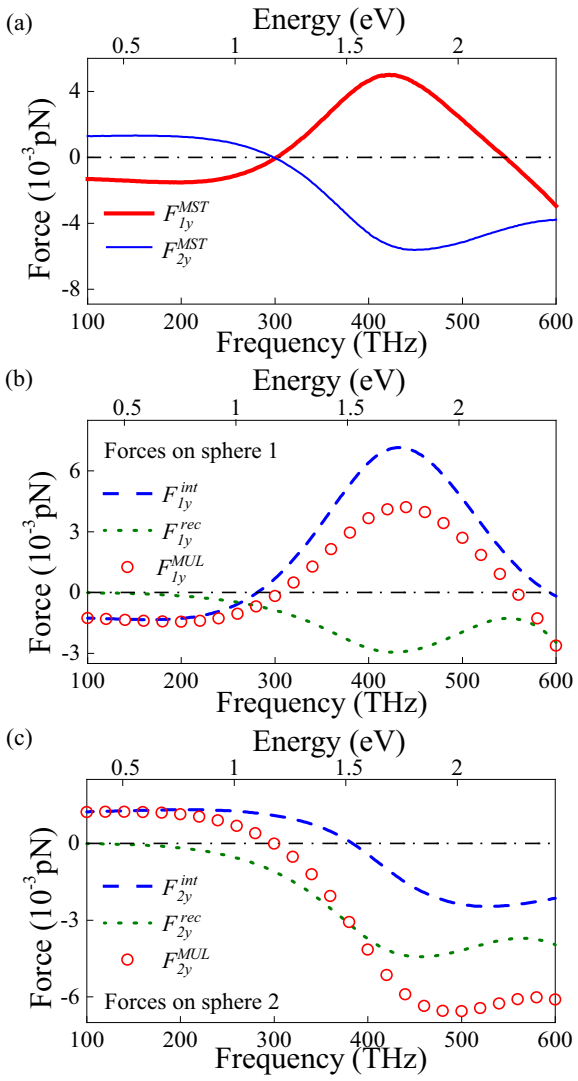

FIG. 3. (a) Lateral optical forces exerted on sphere 1 and sphere 2 in a double-sphere system versus frequency and energy. They are calculated directly from Maxwell's theory and are represented by red thick and blue thin lines, respectively. (b) and (c) The interception force F_y^{int}, the recoil force F_y^{rec}, and the total force $F_y^{\text{MUL}} = F_y^{\text{int}} + F_y^{\text{rec}}$ exerted on sphere 1 and sphere 2 versus frequency and energy. These forces are calculated through the multipole-expansion method. The center-to-center distance in the double-sphere system is $D = 0.3$ μm. The incident light is a circularly polarized evanescent wave ($p = \sqrt{2}/2$, $q = \sqrt{2}i/2$).

IV. LINEARLY DIAGONALLY POLARIZED EVANESCENT-WAVE CASE

A linearly diagonally polarized evanescent wave ($p = q = \sqrt{2}/2$) carries pure transverse SAM [2,8]. It has been established that the lateral optical force F_y exerted on an isotropic sphere in such a wave is proportional to the transverse spin. This force originates entirely from the recoil force, as shown in Fig. 4(a).

In the DLP evanescent wave, the imaginary part of the complex Poynting vector also presents asymmetry along the lateral y direction [as indicated by the white arrows in Fig. 4(b)]. This will result in asymmetric scattering in the lateral direction from the sphere [46,48]. Figure 4(c) shows the distribution of backward scattering of an isotropic sphere in a DLP evanescent wave in the y direction. Consequently, similar to that in the CP evanescent wave, each sphere within the double-sphere system experiences a lateral force that includes

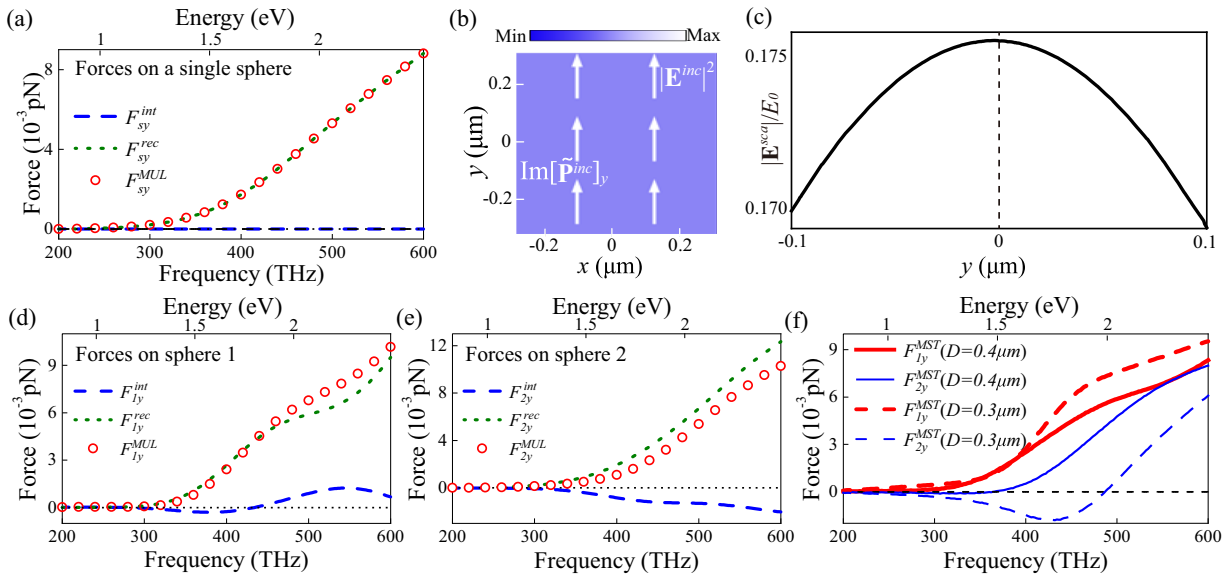

FIG. 4. (a) Lateral optical forces exerted on a single sphere versus frequency and energy. The optical forces are calculated using the multipole-expansion method. (b) The uniform intensity of the incident wave on the xy plane. The white arrows represent the y component of the imaginary part of the incident evanescent wave's complex Poynting vector. (c) The normalized scattered field magnitude ($x = -0.4$ μm) along the y direction to the left of the gold sphere located at coordinates $(0, 0)$ on the xy plane. The frequency of the incident evanescent wave is 350 THz. (d) and (e) Lateral optical forces exerted on the two spheres in a double-sphere system versus frequency and energy. The optical forces are calculated using the multipole-expansion method. The center-to-center distance in the double-sphere system is $D = 0.4$ μm. (f) Lateral optical forces exerted on the two spheres in a double-sphere system versus frequency and energy. They are directly calculated from Maxwell's theory. The solid and dashed lines correspond to center-to-center distances in the double-sphere system of $D = 0.4$ and 0.3 μm, respectively. The incident light is a DLP evanescent wave ($p = q = \sqrt{2}/2$).

not only the recoil force but also the interception force due to asymmetric scattering, as depicted in Figs. 4(d) and 4(e). Moreover, a comparison of the solid red thick and blue thin lines in Fig. 4(f) with those in Fig. 1(b) reveals that the behavior of lateral optical forces experienced by the two spheres in a DLP evanescent wave differs from that in the CP case. In the DLP evanescent wave, the two spheres rarely experience lateral optical forces in opposite directions. Instead, the lateral forces tend to point in the same direction, akin to the trend of the lateral optical force experienced by a single sphere shown in Fig. 4(a). From Figs. 4(d) and 4(e), it is clear that even though the interception force from mutual scattering arises, the recoil force from transverse spin remains dominant. This can be inferred from the distribution of scattered field in the lateral direction [see Fig. 4(c)]. Compared with the CP case [with the same parameters; see Fig. 2(f)], the scattered field distribution in the lateral y direction shows only a slight asymmetry, leaning toward the $-y$ direction. This suggests that the lateral optical force exerted on spheres can be further tuned by changing the incident light's polarization. For instance, if the frequency is fixed as 350 THz, sphere 1 (2) experiences positive (negative) lateral optical forces in the CP case, while both of them become positive when the light is switched to the DLP case.

However, one can still observe the lateral optical force exerted in opposite directions on the two spheres in the DLP case. Their distance needs to be further reduced to enhance the mutual scattering, for instance, reducing the distance from $D = 0.4$ μm to $D = 0.3$ μm as depicted in Fig. 4(f).

V. CONCLUSION

In summary, we investigated the lateral optical forces exerted on a double-sphere system aligned along the propagation direction of an evanescent wave. Through the multipole expansion of optical forces, we found that in contrast to the lateral force on a single sphere, which originates solely from the recoil force due to BSM or transverse SAM, the force on each sphere in the double-sphere system can also come from an interception force. This interception force is induced by asymmetric scattering between the spheres. By modifying the frequency and polarization of the incident evanescent wave, we can adjust the distribution of the interference field formed by the incident and scattered light. This allows for flexible control over the direction of the interception forces and the lateral optical forces exerted on the two spheres, which can be the same or opposite. Moreover, we found that under the same parameters, the asymmetric scattering of an isotropic sphere in a DLP evanescent wave is less apparent than that in a circularly polarized evanescent wave. These conclusions can be extended to systems composed of more spheres (see Sec. I of the Supplemental Material [49] for details). In addition, it should be noted that for the entire double-sphere system, there is no lateral interception force ($F_y^{\mathrm{int}} = 0$) because the incident-plane evanescent wave does not have transverse propagation or a transverse intensity gradient [see Eqs. (3) and (4) for the expression of the interception force]. However, the sum of the interception forces exerted on each sphere is not zero (i.e., $F_{1y}^{\mathrm{int}} + F_{2y}^{\mathrm{int}} \neq 0$). In fact, the total (net) lateral interception force is not equal to

the sum of the interception forces acting on each sphere. That is, $F_y^{\text{int}} \neq F_{1y}^{\text{int}} + F_{2y}^{\text{int}}$, even though it is always true that $F_y = F_{1y} + F_{2y}$. More details can be found in Sec. II of the Supplemental Material [49]. Exploring lateral optical forces in multisphere systems deepens our basic understanding of light-matter interactions. It also has potential applications in particle manipulation, optical sorting, light-driven micro- and nanomotors, and biophysical studies, among others.

ACKNOWLEDGMENTS

We gratefully acknowledge the support from the National Natural Science Foundation of China (Grants No. 12174231 and No. 12074230), the Fundamental Research Program of Shanxi Province through (Grant No. 202103021222001), the Fund for Shanxi 1331 Project, Research Project Supported by Shanxi Scholarship Council of China, and the Program of Education and Teaching Reform in Shanxi Province (Grant No. J20230003).

[1] S. B. Wang and C. T. Chan, Nat. Commun. **5**, 3307 (2014).
[2] K. Y. Bliokh, A. Y. Bekshaev, and F. Nori, Nat. Commun. **5**, 3300 (2014).
[3] F. J. Rodríguez-Fortuño, N. Engheta, A. Martínez, and A. V. Zayats, Nat. Commun. **6**, 8799 (2015).
[4] S. Sukhov, V. Kajorndejnukul, R. R. Naraghi, and A. Dogariu, Nat. Photon. **9**, 809 (2015).
[5] T. H. Zhang, M. R. C. Mahdy, Y. M. Liu, J. H. Teng, C. T. Lim, Z. Wang, and C. W. Qiu, ACS Nano **11**, 4292 (2017).
[6] H. Magallanes and E. Brasselet, Nat. Photon. **12**, 461 (2018).
[7] Y. Z. Shi, T. T. Zhu, J. Q. Liu, D. P. Tsai, H. Zhang, S. B. Wang, C. T. Chan, P. C. Wu, A. V. Zayats, F. Nori, and A. Q. Liu, Sci. Adv. **8**, eabn2291 (2022).
[8] X. N. Yu, Y. X. Li, B. J. Xu, X. G. Wang, L. Zhang, J. Chen, Z. F. Lin, and C. T. Chan, Laser Photon. Rev. **17**, 2300212 (2023).
[9] F. Nan, F. J. Rodríguez-Fortuño, S. Yan, J. J. Kingsley-Smith, J. Ng, B. L. Yao, Z. J. Yan, and X. H. Xu, Nat. Commun. **14**, 6361 (2023).
[10] A. Ashkin, J. M. Dziedzic, J. E. Bjorkholm, and S. Chu, Opt. Lett. **11**, 288 (1986).
[11] E. Fällman and O. Axner, Appl. Opt. **36**, 2107 (1997).
[12] S. Parkin, G. Knüner, T. A. Nieminen, N. R. Heckenberg, and H. Rubinsztein-Dunlop, Opt. Express **14**, 6963 (2006).
[13] F. Peng, B. L. Yao, S. H. Yan, W. Zhao, and M. Lei, J. Opt. Soc. Am. B **26**, 2242 (2009).
[14] Y. C. Li, X. S. Liu, and B. J. Li, Light: Sci. Appl. **8**, 61 (2019).
[15] X. S. Liu, Y. Wu, X. H. Xu, Y. C. Li, Y. Zhang, and B. J. Li, Small **15**, 1905209 (2019).
[16] Y. C. Li, X. S. Liu, X. H. Xu, H. B. Xin, Y. Zhang, and B. J. Li, Adv. Funct. Mater. **29**, 1905568 (2019).
[17] M. H. Alizadeh and B. M. Reinhard, ACS Photon. **2**, 1780 (2015).
[18] H. J. Chen, Y. K. Jiang, N. Wang, W. L. Lu, S. Y. Liu, and Z. F. Lin, Opt. Lett. **40**, 5530 (2015).
[19] A. Hayat, J. P. B. Mueller, and F. Capasso, Proc. Natl. Acad. Sci. USA **112**, 13190 (2015).
[20] Y. Z. Shi, T. T. Zhu, T. H. Zhang, A. Mazzulla, D. P. Tsai, W. Q. Ding, A. Q. Liu, G. Cipparrone, J. J. Sáenz, and C. W. Qiu, Light: Sci. Appl. **9**, 62 (2020).
[21] T. T. Zhu, Y. Z. Shi, W. Q. Ding, D. P. Tsai, T. Cao, A. Q. Liu, M. Nieto-Vesperinas, J. J. Sáenz, P. C. Wu, and C. W. Qiu, Phys. Rev. Lett. **125**, 043901 (2020).
[22] H. S. Shi, H. X. Zheng, H. J. Chen, W. L. Lu, S. Y. Liu, and Z. F. Lin, Phys. Rev. A **101**, 043808 (2020).
[23] D. O'Connor, P. Ginzburg, F. J. Rodríguez-Fortuño, G. A. Wurtz, and A. V. Zayats, Nat. Commun. **5**, 5327 (2014).
[24] A. Y. Bekshaev, K. Y. Bliokh, and F. Nori, Phys. Rev. X **5**, 011039 (2015).
[25] M. Antognozzi, C. R. Bermingham, R. L. Harniman, S. Simpson, J. Senior, R. Hayward, H. Hoerber, M. R. Dennis, A. Y. Bekshaev, K. Y. Bliokh, and F. Nori, Nat. Phys. **12**, 731 (2016).
[26] V. Svak, O. Brzobohatý, M. Šiler, P. Jákl, J. Kaňka, P. Zemánek, and S. H. Simpson, Nat. Commun. **9**, 5453 (2018).
[27] Y. N. Fu, Y. Q. Zhang, C. J. Min, K. W. Fu, and X. C. Yuan, Opt. Express **28**, 13116 (2020).
[28] H. J. Chen, H. X. Zheng, W. L. Lu, S. Y. Liu, J. Ng, and Z. F. Lin, Phys. Rev. Lett. **125**, 073901 (2020).
[29] Z. H. Xiu, Y. S. Zhang, H. S. Shi, H. X. Zheng, H. J. Chen, W. L. Lu, and Z. F. Lin, Phys. Rev. A **104**, 053520 (2021).
[30] M. Nieto-Vesperinas and X. H. Xu, Phys. Rev. Res. **3**, 043080 (2021).
[31] H. B. Xin, Y. C. Li, Y. C. Liu, Y. Zhang, Y. F. Xiao, and B. J. Li, Adv. Mater. **32**, 2001994 (2020).
[32] A. Lehmuskero, P. Johansson, H. Rubinsztein-Dunlop, L. M. Tong, and M. Käll, ACS Nano **9**, 3453 (2015).
[33] S. Barzanjeh, A. Xuereb, S. Gröblacher, M. Paternostro, C. A. Regal, and E. M. Weig, Nat. Phys. **18**, 15 (2022).
[34] J. Yamanishi, H. Yamane, Y. Naitoh, Y. J. Li, N. Yokoshi, T. Kameyama, S. Koyama, T. Torimoto, H. Ishihara, and Y. Sugawara, Nat. Commun. **12**, 3865 (2021).
[35] J. Parker, C. W. Peterson, Y. Yifat, S. A. Rice, Z. Yan, S. K. Gray, and N. F. Scherer, Optica **7**, 1341 (2020).
[36] T. L. Qi, F. Nan, and Z. J. Yan, Adv. Opt. Mater. **11**, 2301158 (2023).
[37] M. A. Ordal, L. L. Long, R. J. Bell, S. E. Bell, R. R. Bell, R. W. Alexander, and C. A. Ward, Appl. Opt. **22**, 1099 (1983).
[38] J. D. Jackson, *Classical Electrodynamics*, 3rd ed. (Wiley, New York, 1999).
[39] R. E. Raab and O. L. de Lange, *Multipole Theory in Electromagnetism* (Oxford University Press, Oxford, 2004).
[40] J. Chen, J. Ng, Z. F. Lin, and C. T. Chan, Nat. Photon. **5**, 531 (2011).
[41] H. J. Chen, S. Y. Liu, J. Zi, and Z. F. Lin, ACS Nano **9**, 1926 (2015).
[42] Y. K. Jiang, H. Z. Lin, X. Li, J. Chen, J. J. Du, and J. Ng, ACS Photon. **6**, 2749 (2019).
[43] H. J. Chen, Q. Ye, Y. W. Zhang, L. Shi, S. Y. Liu, Z. Jian, and Z. F. Lin, Phys. Rev. A **96**, 023809 (2017).
[44] Y. K. Jiang, H. J. Chen, J. Chen, J. Ng, and Z. F. Lin, arXiv:1511.08546.
[45] K. J. Wo, J. Peng, M. K. Prasad, Y. Z. Shi, J. S. Li, and S. B. Wang, Phys. Rev. A **102**, 043526 (2020).

[46] M. Nieto-Vesperinas, J. J. Sáenz, R. Gómez-Medina, and L. Chantada, Opt. Express **18**, 11428 (2010).
[47] M. Born, E. Wolf, and E. Hecht, Phys. Today **53**(10), 77 (2000).
[48] Y. Zhou, X. H. Xu, Y. N. Zhang, M. M. Li, S. H. Yan, M. Nieto-Vesperinas, B. J. Li, C. W. Qiu, and B. L. Yao, Proc. Natl. Acad. Sci. USA **119**, e2209721119 (2022).
[49] See Supplemental Material at http://link.aps.org/supplemental/10.1103/PhysRevA.109.053505 for (1) the lateral optical force in the three-sphere system and the four-sphere system and (2) the inequality between the sum of the interception force on each sphere in a double-sphere system and the interception force on the entire system, which includes Refs. [18,22].